

Ab-initio-NEGF Fundamental Roadmap for Carbon-Nanotube and Two-Dimensional-Material MOSFETs at the Scaling and V_{DD} Limit

Aryan Afzalian
imec, Kapeldreef 75, 3001
Leuven, Belgium
aryan.afzalian@imec.be

Abstract— Using accurate Hybrid-Functional DFT coupled with the Non-Equilibrium Green's function (NEGF) formalism, we explore and benchmark the fundamental scaling limits of CNT-FETs against Si and 2D-material MoS₂ and HfS₂ Nanosheets, highlighting their potential for gate length (L) and supply voltage (V_{DD}) scaling down to 5 nm and to 0.5 V, respectively. The highest drive current is achieved by CNT-FETs with sub 1.3 nm diameters down to $L = 9$ nm and using V_{DD} in the 0.45-0.5V range. Below $L = 9$ nm, however, the HfS₂ NS offers the best drive and could further scale down to $L = 5$ nm with a reduced V_{DD} of 0.5 V.

Keywords— CNT, TMDC, 2D material, DFT, NEGF, CMOS

I. INTRODUCTION

Low-dimensional (LD) materials such as 2D transition-metal dichalcogenides (TMDC) or carbon nanotubes (CNTs) are explored as Si replacement for nanoscale CMOS [1], [2], [3]. In these aggressively scaled materials and devices, quantum effects such as quantum confinement (QC), tunneling and atomistic nature strongly dominate electronic properties and transport, so that efficient, ab-initio, atomistic simulation methods are best suited to model their properties [4]. Using hybrid-functional (HF) density functional theory (DFT), which is essential to accurately capture the CNT bandgap (E_G), coupled with NEGF transport, we investigate the scaling performance of zigzag CNT-FETs made of 4 different (n,0) chirality ($n = 10, 14, 16$ and 19) and benchmark them against Nanosheet (NS) transistors made of Si and 2 monolayer TMDC materials – one, MoS₂, is well-studied with predicted fundamental drive similar to that of Si; the other, HfS₂, is an emerging 2D material with an enhanced fundamental drive current [2], and for which an industry-compatible (ALD) fabrication process was recently demonstrated [5]. Our results further offer a fully ab-initio roadmap for ultra-scaled LD-material CMOS, i.e., a possible fundamental path towards gate-length, L , reduction down to 5 nm and supply voltage, V_{DD} , scaling down to 0.5 V.

II. METHODS

To compute the DFT-based Hamiltonian (H) and relaxed supercell geometries of the Si NS and CNT-FETs, we employed the DFT Package CP2K [6], using a double Zeta (DZVP) atomic-orbital basis, meta generalized gradient approximation (meta-GGA) and the PBE0-TC-LRC HF [7], with 25% of Hartree-Fock exchange and 75% PBE, in order to get an accurate E_G (as fully described in [8]). For MoS₂ and the higher-mobility HfS₂ TMDC, we used QUANTUM ESPRESSO [9] and the generalized gradient approximation (GGA) with the optB86b exchange-correlation functionals

[10], followed by a Wannierization step, as fully described in [2]. The resulting supercell information are then used in our quantum transport (QT) solver, ATOMOS to perform the self-consistent NEGF calculations, using a real-space H for the TMDC NS [2], [8], and a mode-space H for the Si NS and CNT-FETs [4], [11]. Electron-phonon scattering (e-ph) is included within the self-consistent Born approximation, using the deformation potential (DP) theory. We included the dominant acoustic and optical modes, as well as the polar optical mode in the case of the HfS₂ NS [2], [8]. For the 2D materials, we used the parameters described in [2], for the CNT the parameters from [12], while for Si, we used the parameter described in [13].

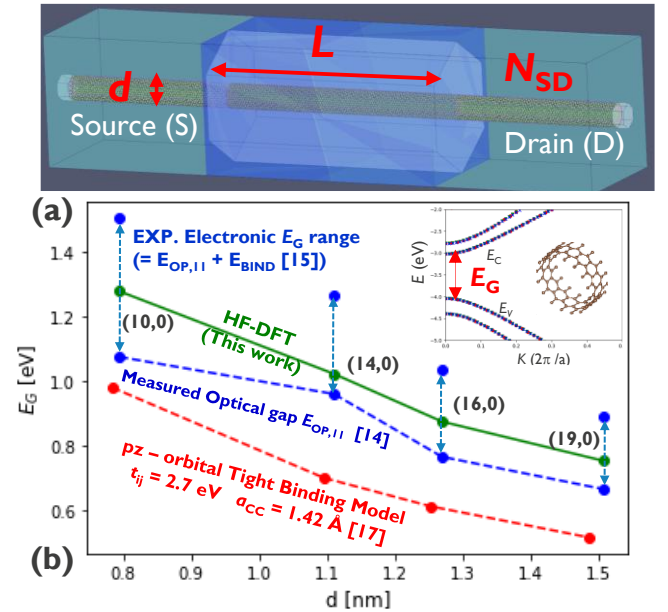


Fig. 1. (a) Atomistic view of a HF-DFT-NEGF simulated CNT-FET with gate length L , S&D extension doping N_{SD} and diameter d . The cylindrical gate with an HfO₂ gate oxide of thickness $t_{OX} = 2$ nm and relative permittivity $\epsilon_R = 15.6$, as well as spacer oxide ($\epsilon_R = 4$) are also shown. (b) Comparison of E_G vs. d relationship obtained from experiments and various models for the zigzag CNT chirality as indicated on the figure for the CNT chirality of Table I. The inset shows the atomic structure and the EK dispersion of a (14,0) CNT slab computed from our real-space (red) and mode-space (blue) DFT-NEGF models. A perfect agreement can be seen.

III. RESULTS

Owing to their inherent nm-scale diameter, d , and high mobility, CNT-FETs are envisioned as high-performance (HP) nanoscale devices [3]. The desired high on current, I_{ON} , that could further enable a V_{DD} reduction down to

approximately 0.5V, is hampered by their large band-to-band tunneling (BTBT) minimum leakage-current limit (I_{MIN}), arising from their low E_G . Fig. 1a defines the simulated CNT-FET geometry. TABLE I. and Fig. 1b show the chirality, d , and E_G extracted from our HF-DFT simulations. In Fig. 1b, our results are further compared to experimental and tight-binding (TB) model results [14], [15]. In a CNT, the electronic E_G is larger than the optically measured gap, $E_{\text{OP},11}$, by the large exciton binding energy $E_{\text{BIND}} (> 100 \text{ meV})$, arising from many body effects. E_{BIND} is, however, not directly measurable, and further sensitive to the dielectric environment and values differ between extraction models [14], [15], [16]. From the modelling side, however, TB models are known to underestimate E_G by about 0.3 eV and lead to $E_G < E_{\text{OP},11}$ ([14] and Fig. 1b), as they neglect these many-body effects. Similarly, traditional DFT methods fundamentally underestimate E_G . HF DFT methods, on the other hand, are well-known to provide accurate E_G descriptions, including for CNTs [16], [17], at the expense of computational costs. Our HF-DFT simulated E_G values are in the expected experimental windows with $E_G > E_{\text{OP},11}$ [14], and in good agreement with those from [16] and [17] that uses HF-DFT but with different HF functionals.

TABLE I. SUMMARY OF THE CNT CHIRALITY, DIAMETERS, AND BANDGAPS, WE COMPUTED USING HF DFT (PBE0-TC-LRC).

Chirality	d (nm)	E_G (eV)
(10,0)	0.794	1.276
(14,0)	1.111	1.020
(16,0)	1.270	0.874
(19,0)	1.508	0.752

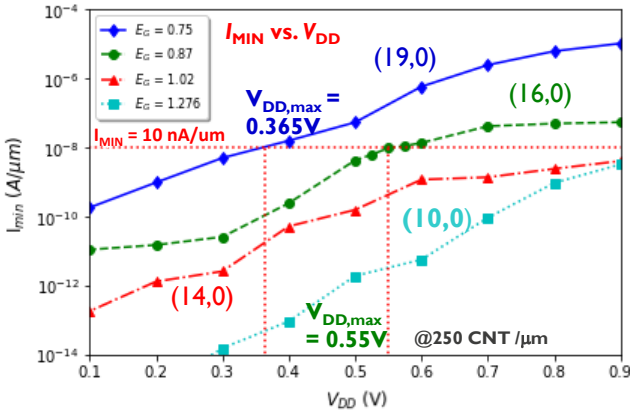


Fig. 2. CNT-FET DFT-NEGF current vs. V_{DD} . (a) BTBT-limited leakage current I_{MIN} vs. V_{DD} for the 4 studied zigzag chirality. $L = 14 \text{ nm}$. $N_{\text{SD}} = 2 \times 10^{20} \text{ cm}^{-3}$. The current is normalized per device width, assuming a typical CNT density of 250 CNT/ μm [3].

Accurate E_G modelling, coupled with a dissipative QT formalism like NEGF, is essential to assess the fundamentals of CNT transistors, including I_{MIN} . To date, however, TB-NEGF models have been used to predict the electrical performance of CNT-FETs [3], [12]. While it might be possible for such models to match experimental E_G - I_{MIN} values by using a smaller d than in the experiments and finetuning the TB parameters, the predicted d - I_{MIN} relationship is hence quite inaccurate, while this is important for practical technology selection. To the best of our knowledge, the

investigation of the fundamentals of CNT-FETs using more accurate HF-DFT NEGF simulations has never been reported.

The relation between I_{MIN} and V_{DD} is investigated using our HF-DFT NEGF model in Fig. 2 for the 4 different zigzag CNT chirality in a n-type $L = 14 \text{ nm}$ FET assuming a CNT density of 250/ μm [3]. Simulated drain-current gate-voltage, $I_D(V_G)$, characteristics of the n-type CNT (16,0) for different V_{DD} are also shown in Fig. 3a. Due to BTBT, in off-state, it is not possible to reduce I_D below I_{MIN} , when decreasing V_G . I_{MIN} increases with V_{DD} for a given E_G .

Direct (ballistic) BTBT from drain (D) to channel (CH) is enabled when D conduction band, E_C , is aligned with the CH valence band, E_V , i.e., when $V_{\text{DD}} \geq V_{\text{DBTBT}}$ with:

$$V_{\text{DBTBT}} = (E_G - E_{\text{CB}}) / q, \quad (1)$$

where E_{CB} is the channel to source barrier required to reach a given off-current level, I_{OFF} . Assuming a typical on-current, I_{ON} , to I_{OFF} ratio of about 10^5 (Fig. 3b):

$$E_{\text{CB}} \approx 5 * K_B * T * \log(10) \approx 0.3 \text{ eV} \quad (2)$$

In such case, the BTBT current, I_{BTBT} , is strong and I_{MIN} -(V_{DD}) typically saturates to its maximum. Additionally, a strong direct I_{BTBT} induces a hole charge pile-up in CH that pins E_C , severely degrading SS (Fig. 3a). At lower V_{DD} , phonon-assisted BTBT takes over (Fig. 3c), enhanced by the large E_{OP} ($\approx 180 \text{ meV}$) in a CNT [12], and the tunnelling probability, hence I_{MIN} , decreases with V_{DD} (Fig. 2).

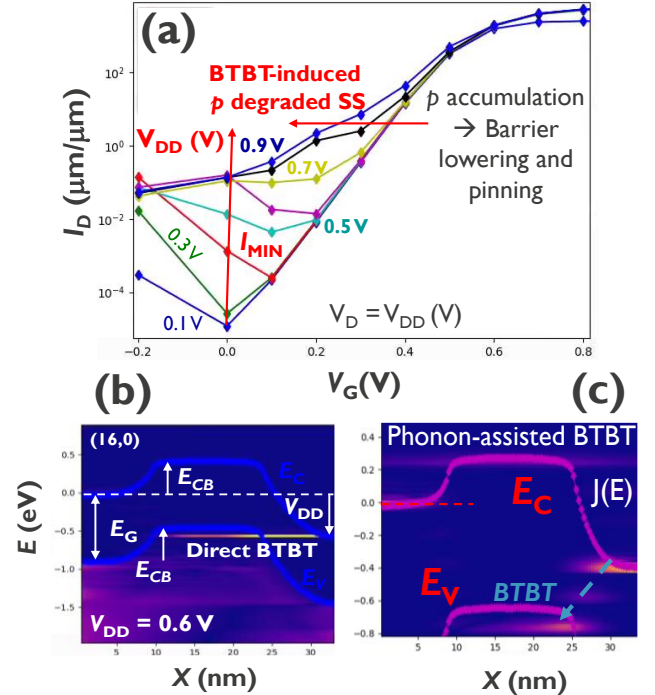


Fig. 3. (a) DFT-NEGF-simulated $I_D(V_G)$ characteristics for the (16,0) CNT-FET vs. V_{DD} . I_{MIN} increases with V_{DD} . A severe SS degradation due to hole pile-up in the channel is also observed when $V_{\text{DD}} > V_{\text{DBTBT}} = 0.57 \text{ V}$ (1). HF-DFT-NEGF-simulated E_C , E_V , and current spectrum, $J(E)$, vs. channel direction, x , for the (16,0) CNT-FET at $V_G = 0$ (OFF-state) with (b) $V_{\text{DD}} = 0.6 \text{ V}$ and (c) $V_{\text{DD}} = 0.4 \text{ V}$. In (b), respectively in (c), V_{DD} is larger (smaller) than V_{DBTBT} , and the drain E_C overlaps (does not overlap) in energy with the channel E_V and direct (respectively, phonon-assisted) BTBT is present. $E_{\text{CB}} \approx 0.3 \text{ eV}$ is the source to channel barrier required to get a typical $I_{\text{ON}}/I_{\text{OFF}}$ ratio of 10^5 . $L = 14 \text{ nm}$. $N_{\text{SD}} = 2 \times 10^{20} \text{ cm}^{-3}$.

For a given I_{OFF} , $V_{\text{DD,max}}$, the maximum V_{DD} to keep $I_{\text{MIN}} \leq I_{\text{OFF}}$ can be inferred from the $I_{\text{MIN}}(V_{\text{DD}})$ curves. For a typical $I_{\text{OFF}} = 10 \text{ nA}/\mu\text{m}$, $V_{\text{DD,max}} = 0.35 \text{ V}$ for a CNT (19,0), 0.55 V for a (16,0) and larger than 1.1 V for the (14,0) and (10,0) case at $N_{\text{SD}} = 2 \times 10^{20} \text{ cm}^{-3}$ (Fig. 2). The corresponding extracted I_{ON} versus V_{DD} are shown on Fig. 4. For the (19,0) case, the too low E_{G} induces a low $V_{\text{DD,max}}$ and SS degradation, so that I_{ON} is limited to about $1000 \mu\text{A}/\mu\text{m}$. For the other studied chirality, however, I_{ON} exceeds $I_{\text{ON,HP-5nm}}$, the HP drive current for the 2037 IRDS node [1], for $V_{\text{DD}} > 0.4 \text{ V}$. The (16,0) CNT-FET reaches the highest $I_{\text{ON}} = 4000 \mu\text{A}/\mu\text{m}$ at $V_{\text{DD}} = 0.5 \text{ V}$, enabling HP logic at $V_{\text{DD}} \leq 0.5 \text{ V}$.

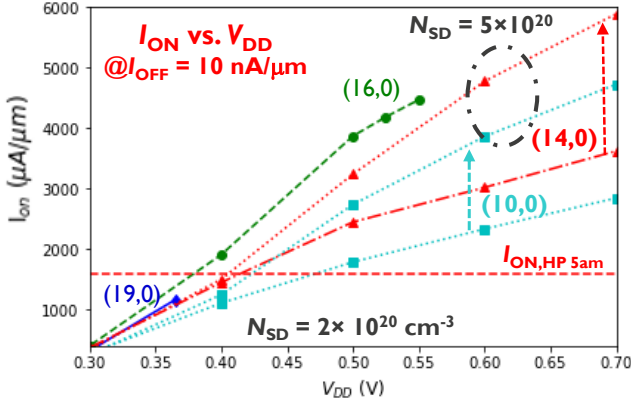


Fig. 4. DFT-NEGF simulated CNT-FET I_{ON} vs. V_{DD} and zigzag chirality at fixed $I_{\text{OFF}} = 10 \text{ nA}/\mu\text{m}$. $L = 14 \text{ nm}$. $N_{\text{SD}} = 2 \times 10^{20} \text{ cm}^{-3}$ if not stated otherwise. CNT density = 250 CNT/ μm .

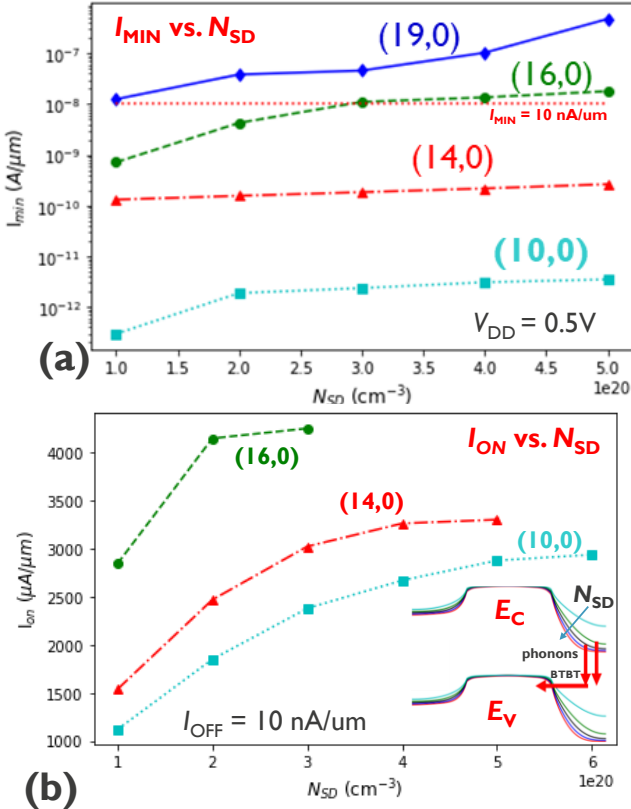


Fig. 5. CNT-FET DFT-NEGF computed current vs. N_{SD} per chirality. (a) I_{MIN} and (b) I_{ON} vs. N_{SD} ($I_{\text{OFF}} = 10 \text{ nA}/\mu\text{m}$) for $L = 14 \text{ nm}$ CNT FETs. The inset shows the (16,0) CNTFET simulated band edges and the related shortening of the BTBT tunneling distance at channel drain-side when increasing N_{SD} . $V_{\text{DD}} = 0.5 \text{ V}$. CNT density = 250 CNT/ μm .

Furthermore, an optimal N_{SD} exists for each chirality. This is shown on Fig. 5 that study the impact of N_{SD} on the $I_{\text{MIN}} - I_{\text{ON}}$ trade-off at $V_{\text{DD}} = 0.5 \text{ V}$. Lowering N_{SD} increases the tunnelling distance at D-side, hence, reduces I_{MIN} (Fig. 5a). On the other hand, lowering N_{SD} below a few 10^{20} cm^{-3} , i.e., the threshold to get E_{C} degenerately doped, strongly affects I_{ON} , as source starvation is observed for lower N_{SD} values (Fig. 5b). In the (16,0) case, $N_{\text{SD}} = 2 \times 10^{20} \text{ cm}^{-3}$ ($= 0.25 \text{ nm}^{-1}$) is close to optimal and there is not much margin to increase it for the targeted I_{OFF} . For the (14,0) and (10,0) cases, on the other hand, increasing N_{SD} to $5 \times 10^{20} \text{ cm}^{-3}$ (i.e., respectively 0.5 and 0.25 nm^{-1}) allows to further increase I_{ON} to 3000 and 2600 $\mu\text{A}/\mu\text{m}$ (Fig. 5b). The (14,0) I_{ON} could reach 5000 and 6000 $\mu\text{A}/\mu\text{m}$ at $V_{\text{DD}} = 0.55$ and 0.6 V respectively, while maintaining I_{OFF} (Fig. 4).

Finally, at fixed N_{SD} and V_{DS} , BTBT, hence, I_{MIN} increases when scaling L due to the increased electric field (Fig. 6). For the (16,0) CNT, I_{MIN} stays below $10 \text{ nA}/\mu\text{m}$ down to $L = 9 \text{ nm}$ at $V_{\text{DD}} = 0.5 \text{ V}$ and $N_{\text{SD}} = 2 \times 10^{20} \text{ cm}^{-3}$, while the (14,0) (respectively the (10,0)) CNT can maintain the same I_{MIN} down to $L = 6$ (respectively $L \leq 4$) nm, using $N_{\text{SD}} = 5 \times 10^{20} \text{ cm}^{-3}$. For comparison, we also simulated the HfS_2 NS I_{MIN} versus L . It is similar to that of the CNT (10,0) and stays below $10 \text{ nA}/\mu\text{m}$ down to $L = 4 \text{ nm}$.

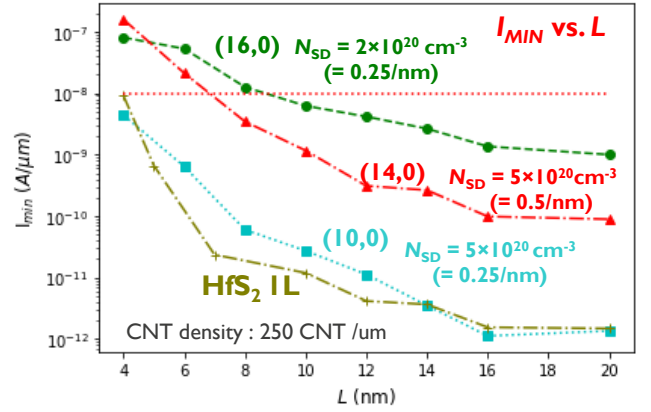


Fig. 6. DFT-NEGF simulated I_{MIN} vs. L at optimal N_{SD} (as indicated on the plot). The HfS_2 1L I_{MIN} ($E_{\text{G}} = 1.202 \text{ eV}$) is also shown. $V_{\text{DD}} = 0.5 \text{ V}$. CNT density = 250 CNT/ μm .

Finally, Fig. 7 benchmarks the L and V_{DD} scaling potential of the CNT-FETs against 2D material MoS_2 and HfS_2 NS [2] and a 4.4-nm-thin Si NS. In term of short-channel effects, the 2D materials achieve the best SS scaling, followed by the CNTs and then Si (Fig. 7b). The highest I_{ON} is achieved by the CNT-FETs down to $L = 9 \text{ nm}$ ((16,0) is best down to $L = 11 \text{ nm}$, then (14,0) or (10,0)) that could scale down to $L \approx 8 \text{ nm}$ using V_{DD} in the $0.45\text{--}0.5 \text{ V}$ range. Below $L = 9 \text{ nm}$, the HfS_2 NS offers the best drive and could further scale down to $L = 5 \text{ nm}$, also using a reduced $V_{\text{DD}} \approx 0.5 \text{ V}$. MoS_2 could allow for the smallest $L \approx 4 \text{ nm}$ but using a larger $V_{\text{DD}} = 0.6 \text{ V}$. For Si, the $t_{\text{Si}} = 4.4 \text{ nm}$ NS scales down to $L \approx 11 \text{ nm}$ at $V_{\text{DD}} = 0.6 \text{ V}$.

IV. CONCLUSIONS

Using Hybrid-Functional DFT coupled with the Non-Equilibrium Green's function formalism, we explored the fundamental physics and performance of scaled CNT-FETs. Using a HF-DFT Hamiltonian in our NEGF model allowed us to significantly improve the accuracy of the E_{G} vs. d and hence our BTBT, I_{MIN} and I_{ON} predictions, when compared to a TB

or standard DFT NEGF simulations. Using our framework, the CNT I_{MIN} and I_{ON} dependency to d , V_{DD} , doping and L was thoroughly explored.

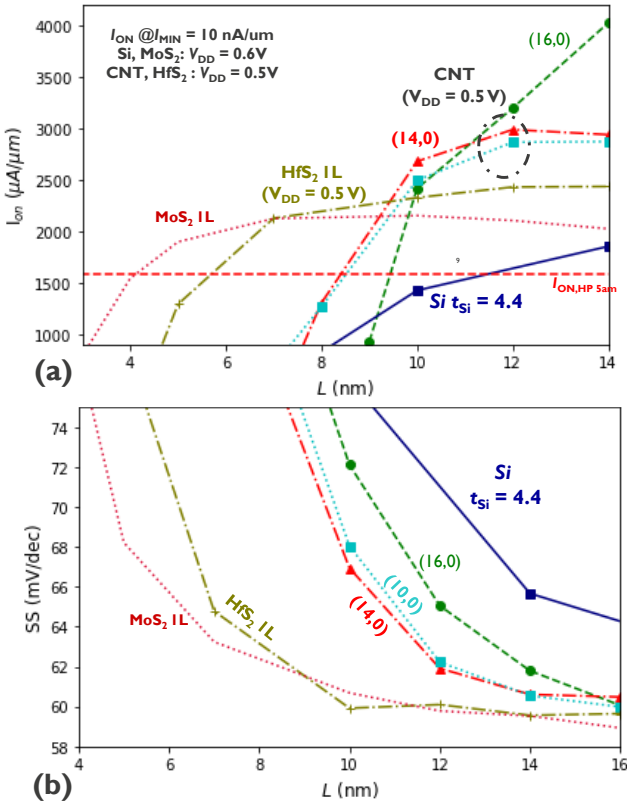


Fig. 7. DFT-NEGF scaling and V_{DD} potential of CNT and 2D-TMDc FETs. (a) I_{ON} vs. L ($I_{\text{OFF}} = 10 \text{ nA}/\mu\text{m}$) and (b) SS vs. L for optimized Si and MoS₂ NS at $V_{\text{DD}} = 0.6 \text{ V}$, as well as high-mobility HfS₂ NS and CNT-FETs at $V_{\text{DD}} = 0.5 \text{ V}$. The highest I_{ON} is achieved by the CNT-FETs down to $L = 9 \text{ nm}$ ((16,0) is best down to $L = 11 \text{ nm}$, then (14,0) or (10,0)) that could scale down to $L \approx 8 \text{ nm}$ using V_{DD} in the 0.45-0.5V range. Below $L = 9 \text{ nm}$, the HfS₂ NS offers the best drive and could further scale down to $L = 5 \text{ nm}$, also using a reduced $V_{\text{DD}} \approx 0.5 \text{ V}$. The current is normalized per device width.

We further benchmarked the fundamental scaling limits of CNT-FETs against 2D material MoS₂ and HfS₂ NS and a 4.4-nm-thin Si NS, highlighting the potential for gate length and supply voltage scaling of these different LD material transistors. Optimized CNT-FETs with $d < 1.3 \text{ nm}$ scales better than Si and are promising candidate for high drive current at reduced V_{DD} of 0.5V down to $L = 8 \text{ nm}$. Owing to their good-transport properties, they achieve the highest I_{ON} down to $L = 9 \text{ nm}$. For lower L , however, the 2D materials feature the best SS, and the HfS₂ NS offers the best drive with a path for scaling down to $L = 5 \text{ nm}$, also using a reduced $V_{\text{DD}} \approx 0.5 \text{ V}$. Overall, our results highlight a fundamental path towards $L = 5 \text{ nm}$, $V_{\text{DD}} = 0.5 \text{ V}$ transistors using high-mobility LD materials.

ACKNOWLEDGMENT

The author acknowledges the Imec Industrial Affiliation Program (IIAP) for funding.

REFERENCES

- [1] IRDS, "IRDS Website". [Online]. Available : <https://irds.ieee.org/editions/2023>.
- [2] A. Afzalian, "Ab initio perspective of ultra-scaled CMOS from 2d material fundamentals to dynamically doped transistors", npj 2D Materials and Applications, 5, 1, 2021.
- [3] Q. Lin *et al.*, "Band-to-Band Tunneling Leakage Current Characterization and Projection in Carbon Nanotube Transistors", ACS Nano, 17, 21, 21083, 2023.
- [4] A. Afzalian, F. Ducry, Pushing the limits of ab-initio-NEGF transport using efficient dissipative Mode-Space algorithms for realistic simulations of low-dimensional semiconductors including their oxide interfaces, *SISPAD*, Kobe, Japan, 305, 2023.
- [5] Mattinen, M.; Popov, G.; Vehkamäki, M.; King, P. J.; Mizohata, K.; Jalkanen, P.; Räisänen, J.; Leskelä, M.; Ritala, M., "Atomic layer deposition of emerging 2D semiconductors, HfS₂ and ZrS₂, for optoelectronics", *Chem. Mater.* **2019**, 31 (15), 5713–5724, DOI: 10.1021/acs.chemmater.9b01688.
- [6] T. D. Kuhne *et al.*, "CP2K: An electronic structure and molecular dynamics software package - Quickstep: Efficient and accurate electronic structure calculations", J. of Chemical Physics, 152, 19, 194103, 2020.
- [7] M. Guidon, F. Schiffmann, J. Hutter and J. VandeVondele, "Ab initio molecular dynamics using hybrid density functionals," J. Chem. Phys., vol. 128, no. 21, p. 214104, 2008.
- [8] A. Afzalian, E. Akhondji G. Gaddemane, R. Duflou and M. Houssa, "Advanced DFT-NEGF Transport Techniques for Novel 2-D Material and Device Exploration Including HfS₂/WSe₂ van der Waals Heterojunction TFET and WTe₂/WS₂ Metal/Semiconductor Contact", in IEEE Transactions on Electron Devices, vol. 68, no. 11, pp. 5372-5379, Nov. 2021, doi: 10.1109/TED.2021.3078412.
- [9] P. Giannozzi *et al.*, "QUANTUM ESPRESSO: a modular and open-source software project for quantum simulations of materials". J. Phys. Condens. Matter., vol. 21, no. 39, p. 395502, 2009. <https://doi.org/10.1088/0953-8984/21/39/395502>.
- [10] J. Klimeš, D. R. Bowler and A. Michaelides, "Chemical accuracy for the van der Waals density functional", J. Phys.: Condens. Matter., vol. 22, p. 022201, 2010.
- [11] A. Afzalian, T. Vasen, P. Ramvall, T.-M. Shen, J. Wu and M. Passlack, "Physics and performance of III-V nanowire broken-gap heterojunction TFETs using an efficient tight-binding mode-space NEGF model enabling million-atom nanowire simulations", J. Phys.: Condens. Matter, vol. 30, no. 25, 254002 (16pp), 2018. <https://doi.org/10.1088/1361-648X/aac156>.
- [12] S. O. Koswatta, *et al.*, Nonequilibrium Green's Function Treatment of Phonon Scattering in Carbon-Nanotube Transistors, *IEEE Trans. Electron Devices*, 54, 9, 2339, 2007.
- [13] A. Afzalian, "Computationally Efficient self-consistent Born approximation treatments of phonon scattering for Coupled-Mode Space Non-Equilibrium Green's Functions", J. Appl. Phys., vol. 110, p. 094517, 2011. <https://doi.org/10.1063/1.3658809>.
- [14] R. B. Weisman, S. M. Bachilo, "Dependence of Optical Transition Energies on Structure for Single-Walled Carbon Nanotubes in Aqueous Suspension: An Empirical Kataura Plot", *Nano Lett.* 3, 9, 1235, 2003.
- [15] J. Deslippe *et al.*, "Electron-Hole Interaction in Carbon Nanotubes: Novel Screening and Exciton Excitation Spectra", *Nano Lett.* 9, 1330, 2009.
- [16] Y. Matsuda *et al.*, "Definitive Band Gaps for Single-Wall Carbon Nanotubes", *J. Phys. Chem. Lett.*, 1, 19, 2946, 2010.
- [17] Manish K Niranjana, "Theoretical investigation of electronic bandgaps of semiconducting single-walled carbon nanotubes using semi-empirical selfconsistent tight binding and ab-initio density functional methods", J. Phys. Commun. 4 015004, 2020.